

Light-polarization and intensity dependence of higher-order nonlinearities in excitonic FWM signals

M. Buck¹, L. Wischmeier², S. Schumacher¹, G. Czycholl¹, F. Jahnke¹, T. Voss², I. Rückmann², and J. Gutowski²

¹ Institute for Theoretical Physics, University of Bremen, 28334 Bremen, Germany

² Institute for Solid State Physics, University of Bremen, 28334 Bremen, Germany

Received 8 July 2004

Published online 14 December 2004 – © EDP Sciences, Società Italiana di Fisica, Springer-Verlag 2004

Abstract. A theory-experiment comparison for the intensity and polarization dependence of spectrally resolved transient four-wave-mixing signals is presented for a ZnSe single quantum well. Results for high intensities deviate from a simple model based on the optical Bloch equations for a five-level system whereas a microscopic theory for coherent excitonic and biexcitonic nonlinearities shows excellent agreement.

PACS. 71.35.-y Excitons and related phenomena – 78.47.+p Time-resolved optical spectroscopies and other ultrafast optical measurements in condensed matter

1 Introduction

The ultrafast coherent dynamics of excitons and biexcitons in semiconductor nanostructures provides a wide field of applications. The manipulation of the excited states leads to remarkable phenomena like lasing without population inversion due to electromagnetically induced transparency (EIT) [1,2] or coherent control of excitons and biexcitons [3–6]. Coherent effects in semiconductors critically depend on their inherent many-particle interactions, which have been extensively studied in the past using transient four-wave mixing (TFWM) [7–13]. For the theoretical description of these effects it is necessary to go beyond approaches developed for atomic systems, like optical Bloch equations (OBE) [14]. Many-particle effects can be systematically included within the semiconductor Bloch equations (SBE) [15]. The ultrafast coherent dynamics is typically influenced by phase-space filling and Hartree-Fock Coulomb effects [7–9], excitation induced dephasing [12,13], and biexcitonic correlations [11,16,17].

In the past, a phenomenological treatment of correlation effects has been used to augment the OBE in order to describe, e.g., the light polarization state of TFWM experiments [18–20] or excitation induced resonance shifts in TFWM [21]. Since the light-polarization dependence is an important aspect of the coherent dynamics, it will be used in this paper as a test for the augmented OBE of reference [20] in comparison with microscopic calculations based on the coherent SBE including biexcitonic correlations. Previous investigations of the polarization dependent TFWM in reference [17] have used a fixed intensity ratio of the two incident pulses. Evaluation of the micro-

scopic theory was in agreement with the experiment. On the other hand, several aspects of recent TFWM experiments using two incident pulses of the same intensity [22] cannot be explained in terms of the augmented OBE for elevated intensities.

In the following we address this problem within a systematic investigation of the intensity dependence of light-polarization selective and spectrally resolved TFWM signals within a direct theory-experiment comparison. Our microscopic model is based on the equations of motion for the excitonic and biexcitonic transition amplitudes in a form that includes all Coulomb effects up to third order in the optical field. In order to correctly describe elevated excitation conditions, the numerical evaluation of this theory is self-consistently extended such that the included excitonic and biexcitonic nonlinearities contribute up to arbitrary order in the field. Within such a treatment only sub-classes of fifth-order and higher nonlinearities are considered. The microscopic calculations reproduce the experimentally observed intensity-dependent appearance of exciton-biexciton oscillations as well as their polarization dependence at higher intensities.

2 Experimental results

A frequency doubled Ti:sapphire laser is used as excitation source for the time-integrated FWM experiments. The laser emits 110 fs pulses at a repetition rate of 82 MHz. The FWM signal is generated by two pulses with variable delay time focused and spatially overlapped on the sample from directions \mathbf{k}_1 and \mathbf{k}_2 . For positive delay time

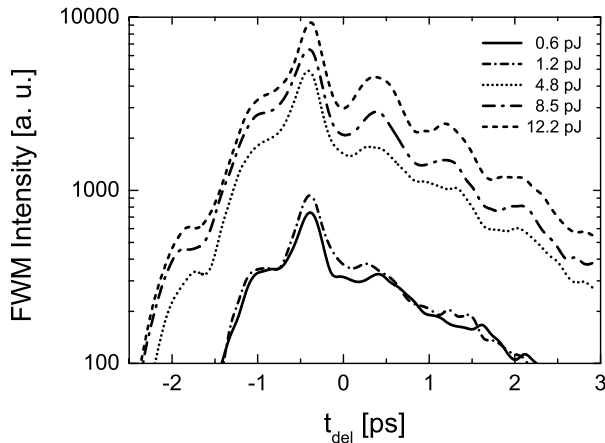


Fig. 1. Experiment: FWM signal vs. delay time for various intensities of the \mathbf{k}_1 pulse at the spectral position of the excitonic resonance. Both pulses are linearly polarized enclosing an angle of $\phi_{\text{pol}} = 75^\circ$. The energy of the \mathbf{k}_1 pulse is varied from 0.6 to 12.2 pJ whereas the energy of the \mathbf{k}_2 pulse is fixed at 12.2 pJ.

the pulse from \mathbf{k}_1 direction precedes the one from \mathbf{k}_2 direction. Both pulses are linearly polarized, with the angle ϕ_{pol} between the polarization vectors. The intensity of each pulse can be varied separately. The FWM signal in direction $2\mathbf{k}_2 - \mathbf{k}_1$ is recorded spectrally resolved by a combination of a spectrometer and a liquid-nitrogen cooled CCD camera. The signal detection is not sensitive to the signal polarization. The central energy of the pulses is set 5 meV below the bound-biexciton resonance to exclusively and resonantly excite the heavy-hole exciton-biexciton system. The light-hole system is shifted to higher energies due to confinement effects and strain. The used 10 nm ZnSe/ZnS_{0.07}Se_{0.93} single quantum well was grown by molecular-beam epitaxy on a GaAs substrate. The sample has been removed from the substrate and mounted onto a glass platelet for experiments in transmission geometry and kept at 4 K in a cryostat.

Figure 1 shows the intensity dependence of the FWM signal at the spectral position of the exciton resonance versus the delay time between the two incident pulses for a polarization angle $\phi_{\text{pol}} = 75^\circ$. For this situation the biexciton contribution to the FWM signal at the exciton is very pronounced. The intensity of the \mathbf{k}_1 pulse is varied while for the intensity of the pulse in \mathbf{k}_2 direction always the largest value is used.

For low intensities of the \mathbf{k}_1 pulse the observed oscillations of the excitonic FWM signal due to simultaneous excitation of excitonic and biexcitonic states only appear for negative delay times t_{del} . This behavior at low intensities is consistent with the model based on the extended OBE in reference [20]. However, at higher intensities the oscillations also emerge for positive delay, which cannot be explained on this level.

In Figure 2 the detected FWM signal for different excitation intensities but equally intense pulses is plotted versus the delay time. For decreasing intensity the oscillations for positive delay times t_{del} are reduced whereas

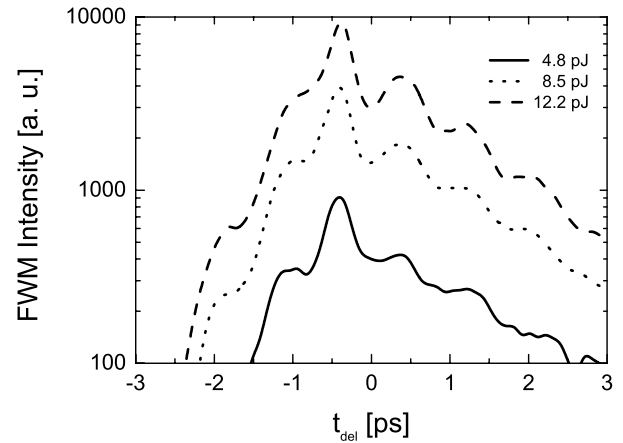


Fig. 2. Experiment: FWM signal vs. delay time for equal intensities of both pulses which are linearly polarized enclosing an angle of $\phi_{\text{pol}} = 75^\circ$. The pulse energies are varied from 4.8 to 12.2 pJ. Signal detection is at the spectral position of the excitonic resonance.

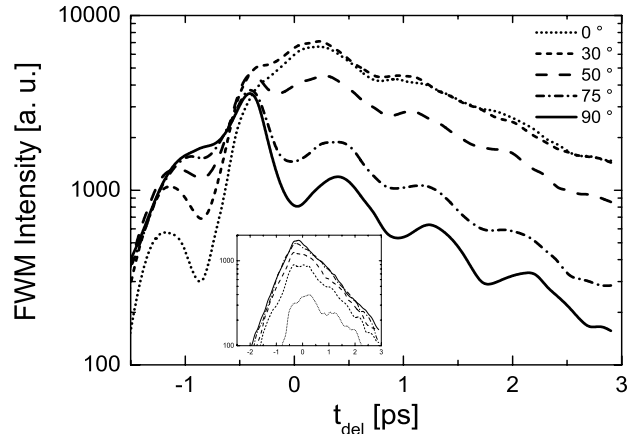


Fig. 3. Experiment: FWM signal vs. delay time for equal intensities at various angles between the linear polarization vectors of the two pulses. Signal detection is at the spectral position of the excitonic (main part) or biexcitonic (inset) resonance. Both pulse energies are fixed at 8.5 pJ.

the structure for negative delay is nearly unchanged. This shows that oscillations for negative delay time appear already in the $\chi^{(3)}$ limit which is reached for small intensities. We find no oscillations at the spectral position of the biexcitonic resonance (not shown).

Results for the variation of the angle ϕ_{pol} between the linear polarization directions of the two pulses from 90° (cross-linear excitation) to 0° (co-linear excitation) at a fixed pulse energy of 8.5 pJ and equal intensity of both pulses for detection at the spectral position of the excitonic (biexcitonic) resonance are displayed in the main part (inset) of Figure 3. For negative delay the exciton-biexciton oscillations disappear when increasing the angle ϕ_{pol} from 0° to 90° , while for positive delay times the oscillations emerge with increasing ϕ_{pol} . Also the strength of the signal strongly depends on ϕ_{pol} . Only slight

oscillations are obtained for detection at the biexciton in the co-linear case.

3 Theory

In the following we summarize the basic ingredients for the theory of coherent optical nonlinearities in quantum wells, applied to a ZnSe system. A solution of Maxwell's equations for the description of the propagating fields requires the macroscopic polarization,

$$\mathbf{P}(t) = \frac{1}{V} \sum_{\mathbf{k}eh} \left[\mathbf{d}^{eh} P_{\mathbf{k}}^{eh}(t) + \mathbf{d}^{eh*} P_{\mathbf{k}}^{eh*}(t) \right], \quad (1)$$

where \mathbf{d}^{eh} is the dipole matrix element between the heavy-hole valence and the conduction band and

$$P_{\mathbf{k}}^{eh} = \langle e_{\mathbf{k}}^{\dagger} h_{\mathbf{k}}^{\dagger} \rangle \quad (2)$$

is the probability amplitude for an electron-hole pair-transition. The operators $e_{\mathbf{k}}^{\dagger}$ ($h_{\mathbf{k}}^{\dagger}$) create an electron (hole) with momentum \mathbf{k} ($-\mathbf{k}$). In addition to the band index, the quantum numbers e, h also indicate the z -component of the electronic total angular momentum. On the level of coherent optical nonlinearities up to third order in the optical field \mathbf{E} [23,24], the dynamics of $P_{\mathbf{k}}^{eh}$ only couples to the biexcitonic transition amplitude,

$$B_{\mathbf{k}_1 \mathbf{k}_2 \mathbf{k}_3 \mathbf{k}_4}^{eh'e'h} = \langle e_{\mathbf{k}_1}^{\dagger} h_{\mathbf{k}_2}^{\dagger} e_{\mathbf{k}_3}^{\dagger} h_{\mathbf{k}_4}^{\dagger} \rangle - \langle e_{\mathbf{k}_1}^{\dagger} h_{\mathbf{k}_2}^{\dagger} \rangle \langle e_{\mathbf{k}_3}^{\dagger} h_{\mathbf{k}_4}^{\dagger} \rangle + \langle e_{\mathbf{k}_1}^{\dagger} h_{\mathbf{k}_4}^{\dagger} \rangle \langle e_{\mathbf{k}_3}^{\dagger} h_{\mathbf{k}_2}^{\dagger} \rangle, \quad (3)$$

which describes correlated four-particle (two-electron-two-hole) transitions beyond the Hartree-Fock (HF) level given by the second and third term on the RHS of equation (3). The equation of motion for $P_{\mathbf{k}}^{eh}$ has the form [25]

$$\begin{aligned} & \left(-i\hbar \frac{\partial}{\partial t} - \epsilon_{\mathbf{k}}^e - \epsilon_{\mathbf{k}}^h \right) P_{\mathbf{k}}^{eh} + \sum_{\mathbf{q}} V_{\mathbf{k}-\mathbf{q}} P_{\mathbf{q}}^{eh} = -\mathbf{d}^{he} \mathbf{E} \\ & + \sum_{e'} \mathbf{d}^{he'} \mathbf{E} \sum_{h'} P_{\mathbf{k}}^{eh'} P_{\mathbf{k}}^{e'h'^*} + \sum_{h'} \mathbf{d}^{h'e} \mathbf{E} \sum_{e'} P_{\mathbf{k}}^{e'h} P_{\mathbf{k}}^{e'h'^*} \\ & + \sum_{\mathbf{q}e'h'} V_{\mathbf{k}-\mathbf{q}} \left[P_{\mathbf{q}}^{eh'} (P_{\mathbf{k}}^{e'h'})^* P_{\mathbf{k}}^{e'h} + P_{\mathbf{k}}^{eh'} (P_{\mathbf{k}}^{e'h'})^* P_{\mathbf{q}}^{e'h} \right. \\ & \quad \left. - P_{\mathbf{q}}^{eh'} (P_{\mathbf{q}}^{e'h'})^* P_{\mathbf{k}}^{e'h} - P_{\mathbf{k}}^{eh'} (P_{\mathbf{q}}^{e'h'})^* P_{\mathbf{q}}^{e'h} \right] \\ & + \sum_{\mathbf{k}'q'e'h'} V_{\mathbf{q}} (P_{\mathbf{k}'}^{e'h'})^* \left[B_{\mathbf{k}+\mathbf{q}, \mathbf{k}'+\mathbf{q}, \mathbf{k}', \mathbf{k}}^{eh'e'h} - B_{\mathbf{k}+\mathbf{q}, \mathbf{k}', \mathbf{k}'-\mathbf{q}, \mathbf{k}}^{eh'e'h} \right. \\ & \quad \left. + B_{\mathbf{k}, \mathbf{k}', \mathbf{k}'-\mathbf{q}, \mathbf{k}-\mathbf{q}}^{eh'e'h} - B_{\mathbf{k}, \mathbf{k}'+\mathbf{q}, \mathbf{k}', \mathbf{k}-\mathbf{q}}^{eh'e'h} \right]. \quad (4) \end{aligned}$$

Considering only the first line of equation (4) the description would be restricted to linear optical properties. The homogeneous part of this line is the momentum-space

Wannier equation for the relative motion of an electron-hole pair under the influence of Coulomb interaction, leading to the excitonic resonances. The remaining terms of equation (4) together with equation (5) account for the optical nonlinearities, which are phase-space filling effects in the coherent limit with $\sum_{\mathbf{k}} P_{\mathbf{k}}^{eh} (P_{\mathbf{k}}^{e'h})^* = f_{\mathbf{k}}^{ee'}$ and $\sum_{\mathbf{k}} P_{\mathbf{k}}^{eh} (P_{\mathbf{k}}^{e'h'})^* = f_{\mathbf{k}}^{h'h}$ (second line of Eq. (4)), Coulomb exchange contributions (third and fourth line of Eq. (4)) and nonlinearities beyond HF. These contributions are determined by the biexcitonic transition amplitude which obeys the equation of motion [25]

$$\begin{aligned} & \left(-i\hbar \frac{\partial}{\partial t} - \epsilon_{\mathbf{k}+\mathbf{q}}^e - \epsilon_{\mathbf{k}'+\mathbf{q}}^{h'} - \epsilon_{\mathbf{k}'}^{e'} - \epsilon_{\mathbf{k}}^h \right) B_{\mathbf{k}+\mathbf{q}, \mathbf{k}'+\mathbf{q}, \mathbf{k}', \mathbf{k}}^{eh'e'h} \\ & - \sum_{\mathbf{q}'} V_{\mathbf{q}'} \left[B_{\mathbf{k}+\mathbf{q}+\mathbf{q}', \mathbf{k}'+\mathbf{q}, \mathbf{k}'-\mathbf{q}', \mathbf{k}}^{eh'e'h} + B_{\mathbf{k}+\mathbf{q}, \mathbf{k}'+\mathbf{q}-\mathbf{q}', \mathbf{k}', \mathbf{k}+\mathbf{q}'}^{eh'e'h} \right. \\ & \quad \left. - B_{\mathbf{k}+\mathbf{q}+\mathbf{q}', \mathbf{k}'+\mathbf{q}+\mathbf{q}', \mathbf{k}', \mathbf{k}}^{eh'e'h} - B_{\mathbf{k}+\mathbf{q}, \mathbf{k}'+\mathbf{q}, \mathbf{k}'+\mathbf{q}', \mathbf{k}+\mathbf{q}'}^{eh'e'h} \right. \\ & \quad \left. - B_{\mathbf{k}+\mathbf{q}+\mathbf{q}', \mathbf{k}'+\mathbf{q}, \mathbf{k}', \mathbf{k}+\mathbf{q}'}^{eh'e'h} - B_{\mathbf{k}+\mathbf{q}, \mathbf{k}'+\mathbf{q}-\mathbf{q}', \mathbf{k}'-\mathbf{q}', \mathbf{k}}^{eh'e'h} \right] \\ & = -V_{\mathbf{q}} (P_{\mathbf{k}}^{eh} - P_{\mathbf{k}+\mathbf{q}}^{eh}) (P_{\mathbf{k}'}^{e'h'} - P_{\mathbf{k}'+\mathbf{q}}^{e'h'}) \\ & \quad + V_{\mathbf{k}-\mathbf{k}'} (P_{\mathbf{k}'+\mathbf{q}}^{eh'} - P_{\mathbf{k}+\mathbf{q}}^{eh'}) (P_{\mathbf{k}}^{e'h} - P_{\mathbf{k}'}^{e'h'}). \quad (5) \end{aligned}$$

The six Coulomb terms of lines 2–4 describe all possible electron-electron, hole-hole and electron-hole interactions of the correlated four-particle states. The last line provides an inhomogeneous source term.

For our numerical calculations, the excitonic and biexcitonic transition amplitudes are expanded in terms of excitonic eigenfunctions $\Phi_n(\mathbf{k})$ according to [25–27],

$$P_{\mathbf{k}}^{eh} = \sum_n P_n \Phi_n(\mathbf{k}), \quad (6)$$

$$\begin{aligned} B_{\mathbf{k}+\mathbf{q}, \mathbf{k}, \mathbf{k}', \mathbf{k}'+\mathbf{q}}^{eh'e'h} & = \sum_{nm} [\Phi_n(\mathbf{k} + \alpha\mathbf{q}) \Phi_m(\mathbf{k}' + \beta\mathbf{q}) B_{nm}^{eh'e'h}(\mathbf{q}) \\ & \quad - \Phi_n(\alpha\mathbf{k}' + \beta\mathbf{k}) \Phi_m(\alpha\mathbf{k} + \beta\mathbf{k}' + \mathbf{q}) B_{nm}^{eh'e'h}(\mathbf{k}' - \mathbf{k})], \quad (7) \end{aligned}$$

where $\alpha = \frac{m_h}{m_e + m_h}$ and $\beta = \frac{m_e}{m_e + m_h}$ contain the electron and hole masses, m_e and m_h , respectively. To reduce the numerical effort only the main contribution of the $1s$ -exciton wavefunction ($n = m = 1$) is included. For a description of FWM experiments, various components of the optical field have to be distinguished. We consider two external optical pulses incoming from directions \mathbf{k}_1 and \mathbf{k}_2 . Optical nonlinearities up to third order lead to additional contributions in the FWM directions $2\mathbf{k}_1 - \mathbf{k}_2$ and $2\mathbf{k}_2 - \mathbf{k}_1$, which is described by the

Fourier decomposition

$$\mathbf{E}(\mathbf{r}, t) = \sum_{\substack{n_1, n_2 = -1 \\ n_1 + n_2 = 1}}^2 \mathbf{E}^{n_1 n_2}(t) e^{i(n_1 \mathbf{k}_1 + n_2 \mathbf{k}_2) \mathbf{r}}, \quad (8)$$

$$P(\mathbf{r}, t) = \sum_{\substack{n_1, n_2 = -1 \\ n_1 + n_2 = 1}}^2 P^{n_1 n_2}(t) e^{i(n_1 \mathbf{k}_1 + n_2 \mathbf{k}_2) \mathbf{r}}, \quad (9)$$

$$B(\mathbf{r}, t) = \sum_{\substack{n_1, n_2 = -2 \\ n_1 + n_2 = 2}}^4 B^{n_1 n_2}(t) e^{i(n_1 \mathbf{k}_1 + n_2 \mathbf{k}_2) \mathbf{r}}. \quad (10)$$

The restrictions for the summation of $P(\mathbf{r}, t)$ and $B(\mathbf{r}, t)$ result from the rotating-wave approximation [27].

Inserting equations (8–10) into the equations for the excitonic and biexcitonic transition amplitude within the excitonic-basis, the contributions are sorted in terms of phase factors $e^{i(n_1 \mathbf{k}_1 + n_2 \mathbf{k}_2) \mathbf{r}}$. While a systematic treatment of higher-order optical nonlinearities would require an extension of the equations of motion (4) and (5), a restricted class of higher-order effects can be obtained from solving equations (4) and (5) self-consistently up to arbitrary order in the optical field. This leads to 4 differential equations for the excitonic transition amplitudes (each direction: \mathbf{k}_1 , \mathbf{k}_2 , $2\mathbf{k}_1 - \mathbf{k}_2$ and $2\mathbf{k}_2 - \mathbf{k}_1$) and 7 differential equations for the biexcitonic transition amplitudes with respect to the restrictions of equations (9) and (10). Finally we have to consider the selection rules along with the polarization of the optical field components. According to the experimental situation we only take into account heavy-hole exciton transitions. Then σ_+ (σ_-) polarized light couples the heavy hole $| -3/2 \rangle$ ($| +3/2 \rangle$) and electron $| -1/2 \rangle$ ($| +1/2 \rangle$) states classified in terms of the z -component of the total angular momentum. We consider all possible circular polarization contributions (obeying to the dipole selection rules) in order to account for arbitrary linear polarization vectors of the incoming light. This leads to 8 equations for P and 28 equations for B which have to be self-consistently solved.

4 Numerical results and discussion

The main parts of the following four figures show the spectrally resolved FWM signal in $2\mathbf{k}_2 - \mathbf{k}_1$ direction at the exciton vs. delay time of the two external pulses. In all figures (except Fig. 6) the two incident pulses are linearly polarized under an angle of 75° .

It has to be mentioned that, as a result of the restriction of the eigenfunction expansion to $1s$ states, the biexciton binding energy is systematically slightly too small. This can be compensated by using a smaller quantum well thickness in comparison to the experiment in order to obtain the appropriate modulation frequencies and the correct spectral positions.

As discussed in Section 2, the experiment reveals oscillations for detection at the exciton and positive time delay which cannot be explained by the extended OBE

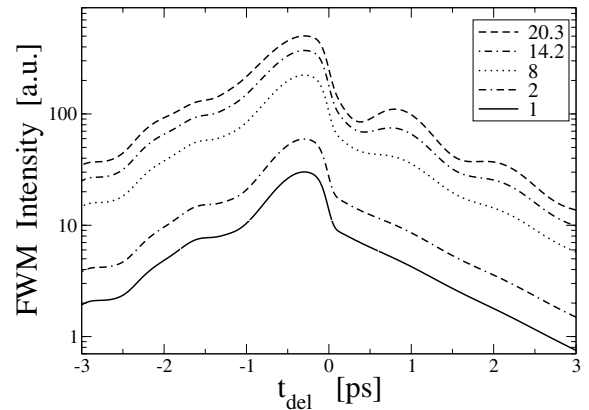


Fig. 4. Theoretical result for the same excitation and detection conditions as in Figure 1 for various normalized intensities of the \mathbf{k}_1 pulse and fixed intensity of the \mathbf{k}_2 pulse. For the dashed line, both pulses have equal intensities. The lowest intensity corresponds to a Rabi energy of $dE/E_B = 2.2 \times 10^{-3}$ in units of the $3d$ excitonic Rydberg energy E_B .

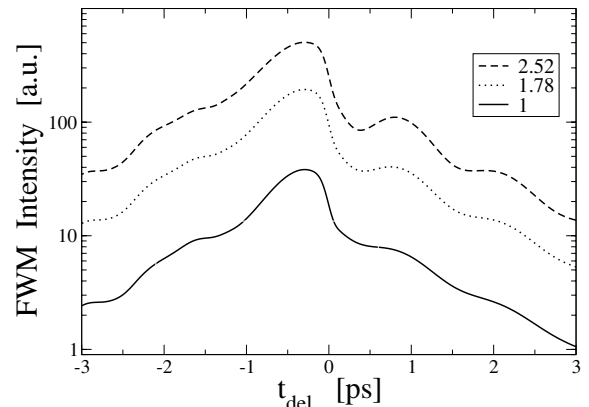


Fig. 5. Theoretical result for the same excitation and detection conditions as in Figure 2. The lowest intensity corresponds to a Rabi energy of $dE/E_B = 6.3 \times 10^{-3}$ in units of the $3d$ excitonic Rydberg energy E_B .

model [22]. The calculation in Figure 4 reproduces this behavior for increasing intensity of the \mathbf{k}_1 pulse while the largest intensity is used for the \mathbf{k}_2 pulse. For reduced intensity of the \mathbf{k}_1 pulse, the oscillations disappear for positive delay but remain for negative delay in agreement with the experimental observation. As discussed in reference [17], the oscillations for negative delay time appear due to third-order effects, while for positive time delay fifth-order nonlinearities lead to beating at higher excitation intensities. There are no oscillations at the biexciton (not shown) for this set of parameters.

In Figure 5 we consider equal intensities of both pulses. For increasing intensity the amplitude of the oscillations for positive delay time is increased, whereas the oscillations remain unchanged for negative delay time. Again, we do not find oscillations at the biexciton resonance (not shown) — which is in agreement with the measurements.

The variation of the angle enclosed between the polarization vectors of the two pulses is shown from 90° to 0°

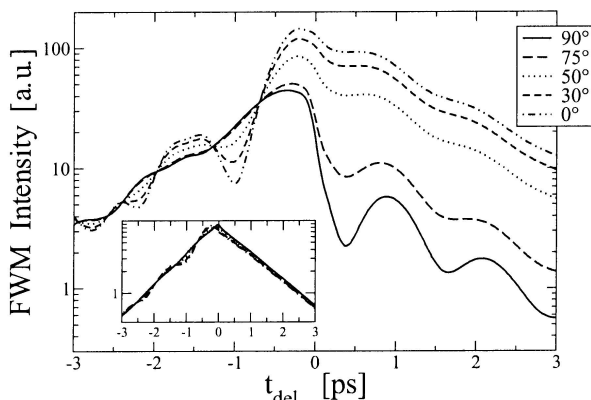


Fig. 6. Theoretical result for the same excitation and detection conditions as in Figure 3 for a Rabi energy of $dE/E_B = 10^{-2}$ in units of the $3d$ excitonic Rydberg energy E_B . Inset shows the FWM signal at the biexciton.

in Figure 6. Cross-linear excitation and $t_{\text{del}} > 0$ leads to oscillations, which are reduced by changing the angle towards zero degrees. The opposite behavior is obtained for negative delay times: from 0° to 90° the oscillations increase in amplitude and show an anharmonic character. Only for 0° the inset shows slight oscillations for detection at the biexciton. While the discussed features are fully consistent with the experimental results of Figure 3, we find deviations in some details. The measured signal for 0° decays more rapidly for increasing negative delay time than for 90° which is not seen in the numerical results. The origin of this difference is unclear and could be due to neglected fifth-order contributions.

Figure 7 shows the phenomenon of excitation induced dephasing. Both pulses have the same intensity. The solid curve is equivalent to the dashed curve of Figure 4. Note that in Figure 5 the intensity is changed only in a relatively small range whereas in Figure 7 the intensity from the lower to the upper curve is increased by a factor of 64. Excitation induced dephasing then leads to a faster decay of the signal at the exciton. At the same time, at the biexciton pronounced oscillations (due to higher-order nonlinearities) start to appear. In present experiments this intensity range was not yet accessible.

5 Summary

Phenomenological models have been suggested in the past to provide a simple and intuitive picture of TFWM signals in semiconductors. In this paper a situation has been analyzed where the augmented OBE model of reference [20] cannot describe various aspects of polarization dependent TFWM signals at higher intensities. We show that a microscopic theory with excitonic and bixcitonic nonlinearities on a self-consistently extended $\chi^{(3)}$ level contains the relevant nonlinearities to reproduce the presented experiments. Deviations of the measured TFWM signals from the augmented OBE model are identified as a result of higher-order nonlinearities.

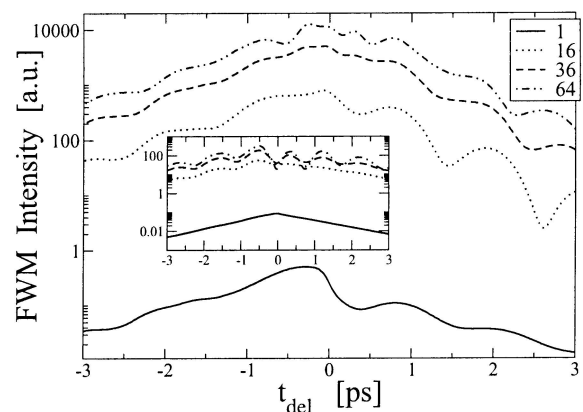


Fig. 7. Theory: FWM signal vs. delay time for equal intensities of both pulses which are linearly polarized with an enclosed angle of 75° of the polarization vectors. For different curves the intensity is changed, the lowest intensity corresponds to a Rabi energy of $dE/E_B = 10^{-2}$ in units of the $3d$ excitonic Rydberg energy E_B . Excitation induced dephasing is observed at the excitonic resonance and oscillations at the biexcitonic resonance (inset) appear for very high intensities.

This work was supported by the Deutsche Forschungsgemeinschaft and with a grant for CPU time at the Forschungszentrum Jülich. The sample has been provided by W. Faschinger, University of Würzburg (deceased 2001).

References

1. M.C. Phillips, H. Wang, I. Rumyantsev, N.H. Kwong, R. Takayama, R. Binder, Phys. Rev. Lett. **91**, 183602 (2003)
2. T. Li, H. Wang, N.H. Kwong, R. Binder, Optics Express **11**, 3298 (2003)
3. A.P. Heberle, J.J. Baumberg, K. Köhler, Phys. Rev. Lett. **75**, 2598 (1995)
4. J. Erland, V.G. Lyssenko, J.M. Hvam, Phys. Rev. B **63**, 155317 (2001)
5. H.G. Breunig, T. Voss, I. Rückmann, J. Gutowski, Phys. Rev. B **66**, 193302 (2002)
6. H.G. Breunig, T. Voss, I. Rückmann, J. Gutowski, V.M. Axt, T. Kuhn, J. Opt. Soc. Am. B **20**, 1769 (2003)
7. K. Leo, M. Wegener, J. Shah, D.S. Chemla, E.O. Göbel, T.C. Damen, S. Schmitt-Rink, W. Schäfer, Phys. Rev. Lett. **65**, 1340 (1990)
8. M. Wegener, D.S. Chemla, S. Schmitt-Rink, W. Schäfer, Phys. Rev. A **42**, 5675 (1990)
9. D.S. Kim, J. Shah, T.C. Damen, W. Schäfer, F. Jahnke, S. Schmitt-Rink, K. Köhler, Phys. Rev. Lett. **69**, 2725 (1992)
10. S. Weiss, M.A. Mycek, J.Y. Bigot, S. Schmitt-Rink, D.S. Chemla, Phys. Rev. Lett. **69**, 2685 (1992)
11. K. Bott, O. Heller, D. Bennhardt, S.T. Cundiff, P. Thomas, E.J. Mayer, G.O. Smith, R. Eccleston, J. Kuhl, K. Ploog, Phys. Rev. B **48**, 17418 (1993)
12. H. Wang, K. Ferrio, D.C. Steel, Y.Z. Hu, R. Binder, S.W. Koch, Phys. Rev. Lett. **71**, 1261 (1993)
13. Y.Z. Hu, R. Binder, S.W. Koch, S.T. Cundiff, H. Wang, D.G. Steel, Phys. Rev. B **49**, 14382 (1994)

14. T. Yajima, Y. Taira, J. Phys. Soc. Jpn **47**, 1620 (1979)
15. H. Haug, S.W. Koch, *Quantum theory of the electronic and optical properties of semiconductors*, 2nd edn. (World Scientific Publishing Co. Pte. Ltd., London, 1993)
16. C. Sieh, T. Meier, F. Jahnke, A. Knorr, S.W. Koch, P. Brick, M. Hübner, C. Ell, J. Prineas, G. Khitrova, H.M. Gibbs, Phys. Rev. Lett. **82**, 3112 (1999)
17. W. Langbein, T. Meier, S.W. Koch, J.M. Hvam, J. Opt. Am. B **18**, 1318 (2001)
18. J.A. Bolger, A.E. Paul, A.L. Smirl, Phys. Rev. B **54**, 11666 (1996)
19. A.L. Smirl, M.J. Stevens, X. Chen, O. Buccafusca, Phys. Rev. B **60**, 8267 (1999)
20. A.L. Smirl, *Coherent exciton dynamics: time-resolved polarimetry*, in *Semiconductor quantum optoelectronics*, edited by A. Miller, M. Ebrahimzadeh, D.M. Finlayson (Institute of Physics Publishing, 1999)
21. J.M. Shacklette, S.T. Cundiff, Phys. Rev. B **66**, 045309 (2002)
22. H.G. Breunig, T. Voss, I. Rückmann, J. Gutowski, Phys. Stat. Sol. (c) **0**, 1445 (2003)
23. M. Lindberg, Y.Z. Hu, R. Binder, S.W. Koch, Phys. Rev. B **50**, 18060 (1994)
24. V.M. Axt, A. Stahl, Z. Physik B **93**, 195 (1994)
25. W. Schäfer, D.S. Kim, J. Shah, T.C. Damen, J.E. Cunningham, K.W. Goossen, L.N. Pfeiffer, K. Köhler, Phys. Rev. B **53**, 16429 (1996)
26. R. Takayama, N.H. Kwong, M. Kuwata-Gonokami, I. Rumyantsev, R. Binder, Eur. Phys. J. B **25**, 445 (2002)
27. W. Schäfer, M. Wegener, *Semiconductor Optics and Transport Phenomena*, 1st edn. (Springer, Berlin, 2002)